Relationship between nanohardness and mineral content of artificial carious enamel lesions

Buchalla, W ; Imfeld, T ; Attin, T ; Swain, M V ; Schmidlin, P R

Abstract: The aim of this study was to compare cross-sectional nanohardness, measured using an ultra-microindentation system, with mineral content, from transversal microradiography, of artificial enamel caries lesions. Sections (85 +/- 10 microm) from 16 bovine enamel samples with artificial caries were prepared. The mineral content and cross-sectional nanohardness at known depths from the surface were compared. Both methods showed lesion profiles with a surface layer. The determination of nanohardness seems limited to lesions with a mineral content >45 vol%. There was a moderate linear relationship between mineral content and the square root of nanohardness (R2 = 0.81). It was concluded that the conversion of cross-sectional hardness into mineral content remains questionable and cannot be recommended.

DOI: https://doi.org/10.1159/000128559

Original Paper

Caries Research

Caries Res 2008;42:157–163
DOI: 10.1159/000128559

Received: February 23, 2007
Accepted after revision: January 2, 2008
Published online: April 29, 2008

Relationship between Nanohardness and Mineral Content of Artificial Carious Enamel Lesions

W. Buchalla[a] T. Imfeld[a] T. Attin[a] M.V. Swain[b] P.R. Schmidlin[a, b]

[a]Department of Preventive Dentistry, Periodontology and Cariology, University of Zurich, Zurich, Switzerland;
[b]Faculty of Dentistry, Biomaterials Unit, University of Otago, Dunedin, New Zealand

Key Words
Caries · Enamel · Hardness · Mineral content · Nanoindentation · Transversal microradiography

Abstract
The aim of this study was to compare cross-sectional nanohardness, measured using an ultra-microindentation system, with mineral content, from transversal microradiography, of artificial enamel caries lesions. Sections (85 ± 10 μm) from 16 bovine enamel samples with artificial caries were prepared. The mineral content and cross-sectional nanohardness at known depths from the surface were compared. Both methods showed lesion profiles with a surface layer. The determination of nanohardness seems limited to lesions with a mineral content >45 vol%. There was a moderate linear relationship between mineral content and the square root of nanohardness ($R^2 = 0.81$). It was concluded that the conversion of cross-sectional hardness into mineral content remains questionable and cannot be recommended.

Depth-related properties of enamel caries lesions can be described in vitro, for example by X-ray attenuation (mineral content profiles) and mechanical characteristics (hardness profiles). Comparative data from microradiography and microhardness measurements are scarce but have shown some correlation [Featherstone et al., 1983; Kielbassa et al., 1999]. The equations for relating microhardness to mineral content provided in these studies differed notably. This indicates that calculation of mineral content from microhardness may not be reliable. So far, no comparison has been made for enamel caries between hardness derived from nanoindentation and mineral content from microradiography. It was the aim of this study to compare nanohardness with mineral content and discuss the reliability of using hardness values to calculate mineral content.

Materials and Methods

Specimen Preparation

One cylindrical specimen (3 mm diameter) was prepared from each of 16 bovine incisors. The enamel surfaces were ground flat with SiC paper and polished up to FEPA P4000 under continuous water-cooling, thereby removing the outer 200 μm. Two strips of adhesive tape (Tesa, Beiersdorf, Hamburg, Germany) were applied parallel to each other on the surface, leaving a 1-mm-wide window. The specimens were immersed in 1 litre of unstirred acidic buffer at 37°C for 6 days in order to create artificial caries-like lesions. This solution contained 3 mmol/l $CaCl_2 \times 2\ H_2O$, 3 mmol/l KH_2PO_4, 50 mmol/l C_2H_5COOH, 6 μmol/l methyldiphosphonate, amounts of KOH to adjust the initial pH to 5.0 and traces of thymol [Buskes et al., 1985].

KARGER

Fax +41 61 306 12 34
E-Mail karger@karger.ch
www.karger.com

0008–6568/08/0423–0157$24.50/0

Accessible online at:
www.karger.com/cre

PD Dr. Wolfgang Buchalla
Universität Zürich, Zentrum für Zahn-, Mund- und Kieferheilkunde
Klinik für Präventivzahnmedizin, Parodontologie und Kariologie
Plattenstrasse 11, CH–8032 Zürich (Switzerland)
Tel. +41 44 634 3383, Fax +41 44 634 4308, E-Mail wolfgang.buchalla@zzmk.uzh.ch

Transversal Microradiography (TMR)

A section was cut with a diamond band saw perpendicular to the exposed surface of the specimens and polished parallel from both cut sides with SiC paper up to FEPA P4000 under continuous water-cooling to a thickness of 85 ± 10 μm. The sections were allowed to dry under ambient conditions. A semi-contact microradiograph of each section together with an aluminium calibration step wedge with 14 steps was taken. High-speed holographic film (SO 253, Kodak AG, Stuttgart, Germany) was exposed with Ni-filtered quasi-monochromatic Cu Kα X-rays (λ = 0.154 nm) from a 1 × 10 mm focus X-ray tube (PW2233/20, Philips/Panalytical, Kassel, Germany) at 20 kV and 20 mA (PW 3830 generator, Philips/Panalytical) for 12 s. The film-focus distance was 40 cm. The developed film was analyzed using a transmitted light microscope with a ×20 objective (Axioplan, Zeiss, Oberkochen, Germany) with a CCD camera (XC-77CE, Sony, Tokyo, Japan) and a PC with framegrabber and data acquisition and calculation software (TMR 1.25e, Inspector Research BV, Amsterdam, The Netherlands). The mineral content (vol%) was calculated from film transmission as a function of specimen depth. The film transmission was measured from the specimen surface towards the deeper enamel within a 350-μm-wide window. The analogue signal from the CCD camera was digitized by a framegrabber (Flashpoint 3D, Integral Technologies, Indianapolis, Ind., USA). The microscope-transmitted light intensity was adjusted so that the pixel grey value resolution of 8 bit could be fully used. The mineral content was calculated from the specimen grey levels using the formula of Angmar et al. [1963], assuming the density of the mineral to be 3.15 kg/l. Calculations used Cu Kα line linear attenuation coefficients of 13.13×10^3 m^{-1} (aluminium), 1.13×10^3 m^{-1} (organic matter/water) [Angmar et al., 1963; de Josselin de Jong et al., 1987] and 26.26×10^3 m^{-1} calculated as suggested elsewhere [Angmar et al., 1963; de Josselin de Jong et al., 1987] by using crystallographic properties of hydroxyapatite and respective atomic absorption coefficients [International tables for X-ray crystallography, 1962; Young and Brown, 1982]. The film grey values were related to the corresponding aluminium thickness by scanning the step wedge area and fitting a fourth-degree polynomial through the data points. To use Angmar's formula, the specimen thickness is also required. It is difficult to reliably measure the thickness of thin enamel sections by mechanical means. Therefore, the enamel thickness was calculated from the grey values within the sound area of the section, and the mineral content was assumed to be 87 vol% [Angmar et al., 1963; de Josselin de Jong et al., 1987]. In order to allow for direct comparison of the TMR data with data from nanoindentation, the mineral content was considered only at steps of 10 μm from 10 to 160 μm distant from the specimen surface, which are the depths where the nanoindentations were placed (see below). The mineral content was averaged from 5 measurement points 1 μm apart at the depth in question to cover a field of similar width as with the nanoindentation, e.g. the mineral content at 10 μm was averaged from 8, 9, 10, 11 and 12 μm.

Nanoindentation

The same samples used for microradiography were mounted on a glass Petri dish using sticky wax. A load and displacement sensing indentation system (Ultra Micro-Indentation System, UMIS-2000, CSIRO, Sydney, Australia) with a 3-sided pyramidal diamond (Berkovich) indenter was used. The indenter contact area versus depth was calibrated using fused silica [Oliver and Pharr, 1992]. Three indentation lines 100 μm apart were carried out in the same demineralized area as TMR was measured. The first indentation of each line was set 10 μm below the enamel surface. The subsequent indentations had a spacing of 10 μm so that the first 10–160 μm below the enamel surface were assessed. The maximal force applied was set at 20 mN. The load function consisted of a 'square root' loading segment of 20 increments each with a delay time of 0.1 s, a holding segment at peak load (10 s) and an unloading segment of 20 increments. The UMIS-2000 software was used to calculate the nanohardness as a function of penetration depth of each indentation. That is, nanohardness (H) was determined from analysis of a polynomial fit to the upper 70% of the unloading component of the force displacement curve via determination of the plastic penetration depth at maximum load, h_p. Thereby $H = F_{max}/A$, where A is the area of contact which is related to h_p via the calibration curve.

Scanning Electron Microscopy

One section was etched with 38.5% phosphoric acid for 5 s, dried with compressed air and sputter coated with gold without additional drying and viewed with a scanning electron microscope (SEM) in secondary electron emission mode (10 kV). Images at different magnifications were saved to computer disc.

Data Analysis

Means, standard deviations and coefficient of variation were calculated from nanohardnesses and mineral contents at every depth (10, 20, … 160 μm). Both nanohardness and its square root (which corresponds to the indenter penetration depth) were plotted against mineral content. Least-squares linear regressions were fitted to the data and the individual 95% prediction intervals were calculated. Statistical calculations were performed using SPSS 11.0 for Mac software.

Results

Mean mineral content and nanohardness profiles from all 16 specimens (fig. 1a) showed that nanohardness profiles represent the mineral-rich surface layer and lesion body in a similar way to TMR but with some significant differences. The shapes of the mean relative mineral content and mean relative nanohardness profiles (i.e. given as a percentage of the averaged sound values between 120 and 160 μm specimen depth) did not differ from the profiles for the absolute data (fig. 1b). The mean coefficient of variation of nanohardness (36%) was higher than that of TMR (4%). The coefficient of variation of nanohardness was higher than that of TMR for every single measurement point (fig. 2). Mineral content was within a range of 45–91 vol% and nanohardness within a range of 0.2–7.3 GPa.

A scatter plot (fig. 3a) showed a non-linear relationship between mineral content and nanohardness. The

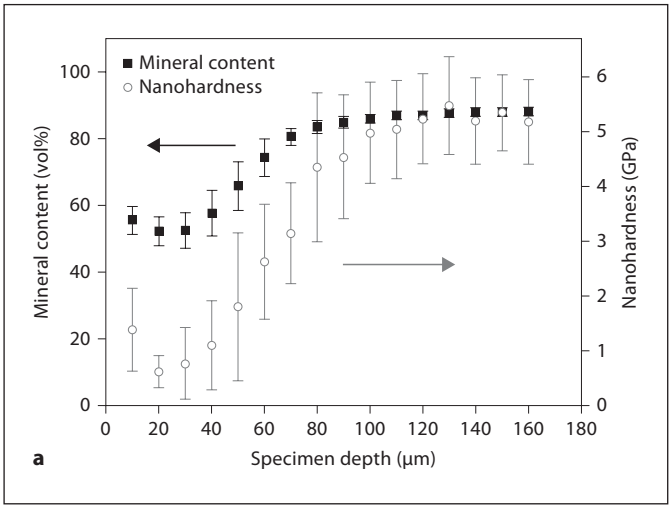

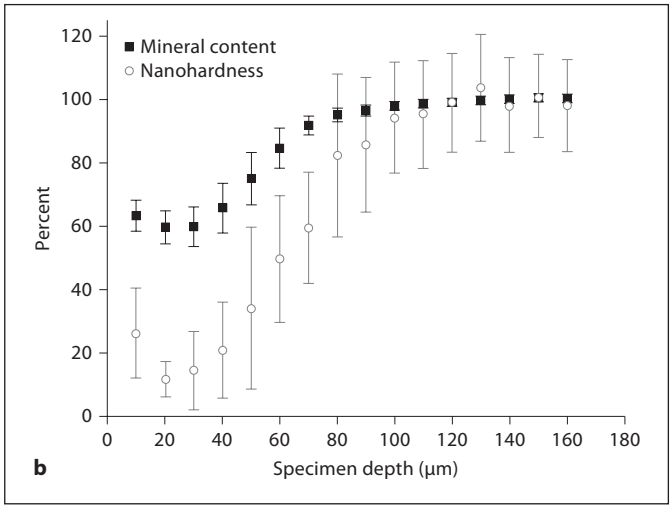

1

Fig. 1. a Profiles of mineral content and nanohardness across the enamel lesion from the surface (0 μm) to sound enamel (160 μm). Means (n = 16) and standard deviations. The arrows refer to the relevant y-axes (black arrow: mineral content; grey arrow: nanohardness). **b** Same as **a** but in relative terms with mineral content and nanohardness as a percentage of sound enamel (100%) calculated from data at 120–160 μm depth.

Fig. 2. Coefficients of variation of mineral content and nanohardness.

Fig. 3. a Scatter plot of nanohardness against mineral content. Data points form a horizontal cluster around 45–70 vol% and a rather vertical cluster around 85–90 vol%. **b** Same as **a** but in relative terms with mineral content and nanohardness as a percentage of sound enamel (100%) calculated from data at 120–160 μm depth.

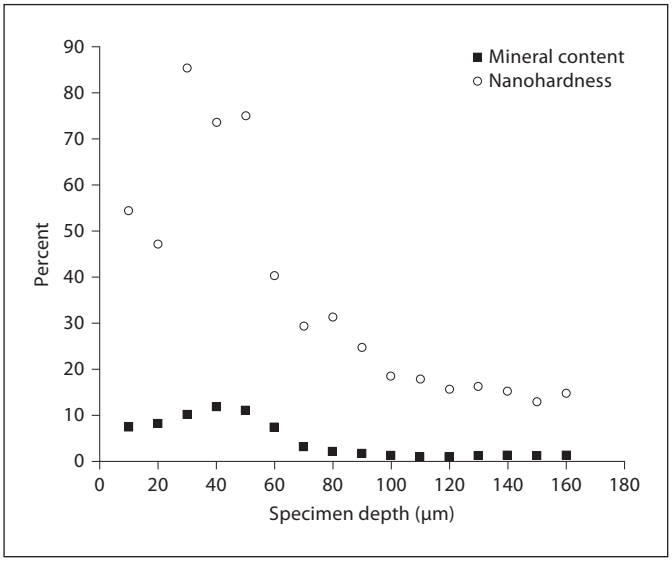

2

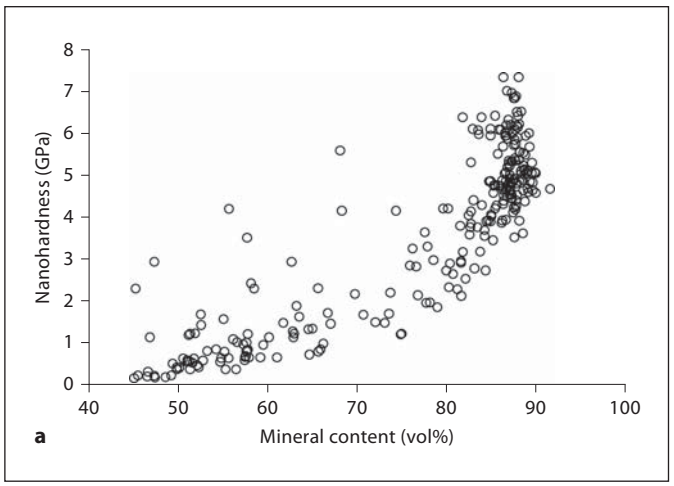

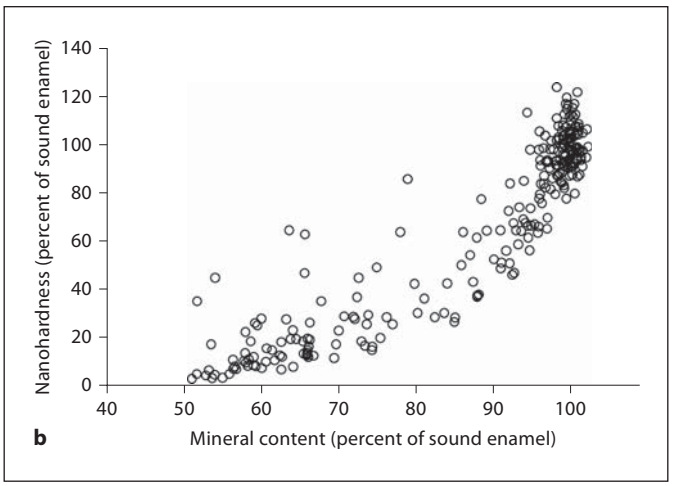

3

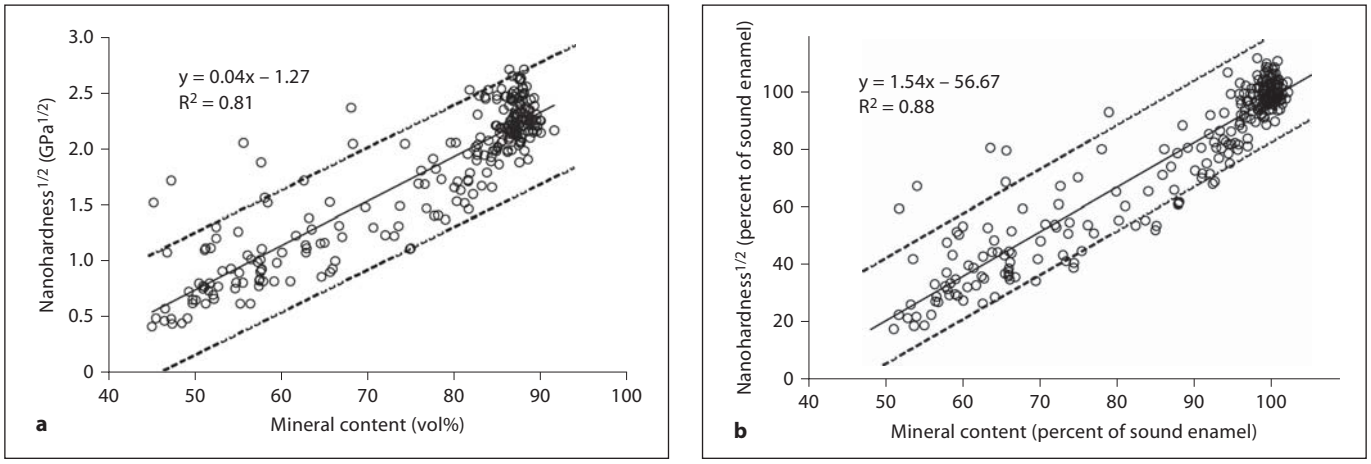

Fig. 4. a Scatter plot of the square root of nanohardness against mineral content. Solid line = Least-squares linear regression; dashed lines = 95% prediction interval boundaries. **b** Same as **a** but in relative terms with mineral content and nanohardness as a percentage of sound enamel (100%) calculated from data at 120–160 μm depth.

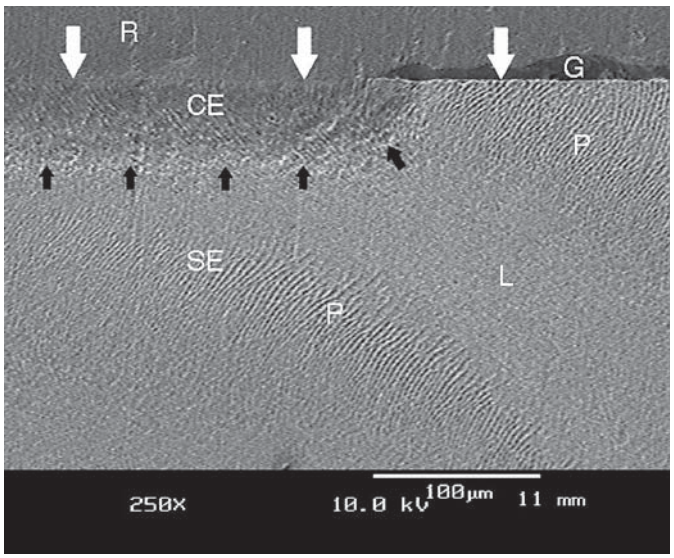

Fig. 5. SEM image of a bovine enamel section with an artificial caries lesion. The white arrows indicate the specimen surface, the black arrows the boundary of the lesion. R = Resin (embedding material); G = gap (artefact); CE = carious enamel (caries lesion); SE = sound enamel; P = prisms cut almost perpendicularly; L = prisms cut almost longitudinally.

plot indicated 2 clusters: 1 at sound values (greater than ca. 85–90 vol% mineral) and 1 around values representing the lesion body (up to ca. 60 vol%). Relative mineral content and relative nanohardness also showed a nonlinear relationship (fig. 3b). The square root of nanohardness (a measure of indentation depth) showed a moderate linear relationship (R^2 = 0.81) with mineral content (fig. 4a). Using the relative data, the square root of nanohardness showed a slightly better fit with mineral content (fig. 4b), but the scatter around the regression line was still high.

A SEM image of 1 section illustrates the artificial caries lesion and typical changes in prism orientation (fig. 5).

Discussion

The thickness of the enamel section has to be known for determination of the mineral content by microradiography [Angmar et al., 1963]. Thickness measurement by mechanical means, e.g. by a micrometer gauge, has only limited accuracy. A micrometer gauge with pointed tips cannot be used because the enamel section may be damaged, which would lead to incorrect values. Using a flat-ended gauge results in measurement of the thickest part of the section and is also limited by the accuracy of the micrometer gauge itself. Another approach would be to measure the edge thickness of the sections under a microscope using a cross-hair ocular, but this method is rather subjective, less precise and reflects the thickness of the edge rather than of the whole section. Therefore, it was decided to calculate the thickness of the sections from the film grey values, corresponding to the aluminium thickness averaged from within a sound area of the enamel. Following this procedure, the mineral content

data were normalized to sound mineral content of human enamel (87 vol%), a value that was determined by chemical means [Angmar et al., 1963; de Josselin de Jong et al., 1987]. The mineral content of sound bovine enamel was assumed to be the same as for sound human enamel because it has been shown that the mineral contents of bovine and human enamel are not significantly different [Edmunds et al., 1988]. The method used is simple and fast, but an error may be introduced, since the real mineral content of a specific section may be slightly higher or lower than 87 vol%. It can be assumed that this error is within the same range as the error introduced by mechanical determination of the section thickness. While smaller differences between the true mineral content of sound enamel and the mineral content value used would not allow this method for the determination of absolute mineral content values of sound enamel, it is suitable for analyzing specimens with demineralized enamel because changes of mineral content of enamel with caries-like lesions are >1 order of magnitude higher.

In order to calculate mineral content from film transmission, the mineral density was assumed to be the same as that of hydroxyapatite: 3.15 kg/l [Angmar et al., 1963]. Other sources report the mineral density of human enamel to be 3.0 kg/l [Elliott, 1997]. Use of the latter density would result in mineral content values being 5% higher. However, normalizing the mineral content data to a sound mineral content of 87 vol%, as was done in this study, eliminates an error made by using a mineral density value that is smaller or higher than the actual mineral density.

The mineral content of enamel decreases from the outer surface towards the inner surface (next to the dentine) [Angmar et al., 1963; Wilson and Beynon, 1989]. These differences may be significant if enamel close to the outer surface is compared to enamel close to the dentine. In the present study, however, the outer 200 μm were removed during specimen preparation and the measurements made were restricted to within 160 μm of this newly created surface. The data from the publications mentioned suggest that within this area a change of mineral content should be small. This is also confirmed in figure 1, where the microradiographic data points beyond 100 μm are on the same level. Additionally, this indicates that the cut and polished sections used in this study had a rather uniform thickness.

Studies to date have reported a wide range of nanohardness values for sound enamel. The nanohardness of sound bovine enamel (our study) was slightly higher than reported for primary enamel (4.88 ± 0.35 GPa) [Mahoney et al., 2000] and human molar enamel (4.75 ± 0.14 GPa) [Barbour et al., 2003]. However, recently values even higher than ours, mostly between 6 and 7 GPa, were reported for human molar enamel [Braly et al., 2007]. All these studies used human enamel, while we used bovine enamel, which tends to be softer than human enamel [Reeh et al., 1995]. Using nanoindentation, human dental enamel was found to be highly inhomogeneous with harder zones at the outer enamel layers than at the inner layers [Cuy et al., 2002], which may contribute to the differences in nanohardness values reported in different studies. Also, it is known that the properties of enamel are very dependent on local prism orientation and mineral content [Spears, 1997]. In addition a more than 2-fold hardness difference was found between the core and the surrounding protein-rich sheath area of enamel prisms [Ge et al., 2005]. The human enamel prism diameter (around 5 μm) [Maj, 1947] and the width of the interprismatic region (1–3 μm) [Scott and Wyckoff, 1946] are in the order of magnitude of the width of the impression of the Berkovich indenter (the impression diameter in this study was in the order of 7–3 μm, the probing depth was 1–0.4 μm). Bovine enamel is known to have thicker crystallites [Arends and Jongebloed, 1978], but exact data on the prism diameter and the interprismatic region have not been published. In SEM images of specimens of this study we found that the prism diameter of bovine enamel is in the order of 3 μm, and interprismatic enamel regions are around 1 μm wide.

A difference between human and bovine enamel is the pattern in which the prisms are packed together, with bovine enamel prisms being arranged in pattern 2 structure, meaning the prisms are orientated parallel to each other in rows with interrow sheets of crystals which are wider than the regions between the prisms within the rows [Boyde, 1965]. The largest proportion of human enamel consists of pattern 3 prism structure, where the prisms are arranged in a more alternating pattern, in a 'horseshoe' or 'keyhole' pattern, where each prism extends between 2 other prisms when looked at perpendicularly to the prism long axis. The bovine enamel used was cut along the long axis of the tooth and, as in human enamel, because of the bending and twisting of the enamel prisms on their way from the dentine-enamel junction towards the outer enamel surface [Radlanski et al., 2001], prism orientation varied on the polished surface of the enamel sections. Prisms were cut from almost perpendicular to rather longitudinal (fig. 5). Differences in enamel microstructure may influence nanohardness measurements in absolute terms. For a comparison of

nanohardness with mineral content applied to demineralized specimens, however, the distribution of the data may be more relevant than absolute hardness values.

The variability of nanohardness was high compared to the mineral content data, which may be partly attributed to the different volumes that were 'probed'. It is conceivable that the small volume probed by the nanoindenter (see above) picked up local differences more easily than the X-ray attenuation, which is averaged through a relatively thick layer of enamel (85 μm). Another reason for the variability, particularly within the lesion itself, of both nanohardness and mineral content, may be that means and standard deviations were calculated from the impressions made in 16 different samples. Although all samples were treated the same way, there are slight differences in mineral content and hardness distribution within the specimen at every given distance from the outer surface. Since all measurements were performed at the same distances from the outer surface in all specimens, variability between the specimens will be reflected in a higher coefficient of variation of both TMR and hardness data.

A close relationship between microhardness (Knoop) and mineral content determined by TMR has been reported with R^2 values of 0.84 and 0.92 between the square root of hardness and mineral content [Featherstone et al., 1983; Kielbassa et al., 1999]. The present study compared mineral content determined by TMR with nanohardness. Although there is a difference in load, impression area and impression depth, the same physical principles apply for micro- and nano-hardness determination. Hardness data are a measure for the projected impression area of an indenter at a given load. Consequently, the square root of hardness corresponds to indenter penetration depth, which shows better, but still not good, correlation with mineral content. A linear least-squares fit (fig. 4) in our opinion does not represent the true relationship between mineral content and hardness. Two rather independent data clusters, in the low and highly mineralized (sound) areas seem to differ in their correlation between mineral content and nanohardness. The lower mineralized cluster showed a smaller slope than the higher mineralized cluster. Microhardness data show the same tendency [Featherstone et al., 1983; Kielbassa et al., 1999].

The lower border of the 95% prediction interval has an X intercept (0 GPa) at 45 vol% (fig. 4a). Therefore, determination of nanohardness has limited reliability in enamel with a mineral content <45 vol%, making lesion assessment with nanohardness questionable in severely demineralized enamel lesions.

It has become increasingly popular to calculate mineral content from microhardness profiles, e.g. by formulas based on the assumption of a linear correlation between square root of microhardness and mineral content given in previous papers [Featherstone et al., 1983; Kielbassa et al., 1999]. However, the clear difference between the formulas given in these studies already suggests caution, as does the more likely non-linear relationship between the square root of microhardness and mineral content and data scatter around 2 clusters. Based on the present results, calculating mineral content from nanohardness cannot be recommended either. Finding a correlation between nanohardness and mineral content is not a mathematical problem. A fit with a correlation coefficient in the order of 0.9 may be found by splitting the data into 2 halves of lower and higher mineral content. Still, it is the data scatter that makes using, for instance, linear regression to calculate mineral content from hardness data unreliable. Converting nanohardness values into mineral content always introduces an additional error to the data and does not add new information.

The cross-sectional properties of caries lesions can be described, among others, in terms of 2 different properties – the mechanical properties (hardness) and the mineral content. Based on the results of this and the papers mentioned, it is not recommended to calculate mineral content from micro- or nano-hardness profiles. If it is important to report mineral content data, microradiography is the method of choice. However, depth profiling of caries lesions using micro- or nano-hardness provides useful information on mechanical properties and structural integrity that, in turn, cannot be determined by mineral content.

Acknowledgement

The authors are grateful to Mr. Felix Schmutz for taking the SEM image.

References

Angmar B, Carlström D, Glas JE: Studies on the ultrastructure of dental enamel. IV. The mineralization of normal tooth enamel. J Ultrastruct Res 1963;8:12–23.

Arends J, Jongebloed W: Crystallites dimensions of enamel. J Biol Buccale 1978;6:161–171.

Barbour M, Parker DM, Allen G, Jandt K: Human enamel dissolution in citric acid as a function of pH in the range 2.30 ≤ pH ≤ 6.30 – a nanoindentation study. Eur J Oral Sci 2003;111:258–262.

Boyde A: The structure of developing mammalian dental enamel; in Stack MV, Fearnhead RW (eds): Tooth Enamel. Its Composition, Properties, and Fundamental Structure. Bristol, Wright & Sons, 1965, pp 163–167.
Braly A, Darnell L, Mann A, Teaford M, Weihs T: The effect of prism orientation on the indentation testing of human molar enamel. Arch Oral Biol 2007;52:856–860.
Buskes JA, Christoffersen J, Arends J: Lesion formation and lesion remineralization in enamel under constant composition conditions: a new technique with applications. Caries Res 1985;19:490–496.
Cuy J, Mann A, Livi K, Teaford M, Weihs T: Nanoindentation mapping of the mechanical properties of human molar tooth enamel. Arch Oral Biol 2002;47:281–291.
De Josselin de Jong E, ten Bosch JJ, Noordmans J: Optimised microcomputer-guided quantitative microradiography on dental mineralised tissue slices. Phys Med Biol 1987;32:887–899.
Edmunds D, Whittaker D, Green RM: Suitability of human, bovine, equine, and ovine tooth enamel for studies of artificial bacterial carious lesions. Caries Res 1988;22:327–336.
Elliott JC: Structure, crystal chemistry and density of enamel apatites; in Chadwick D, Cardew G (eds): Dental Enamel. Chichester, Wiley & Sons, 1997, pp 54–67.
Featherstone JD, Ten Cate JM, Shariati M, Arends J: Comparison of artificial caries-like lesions by quantitative microradiography and microhardness profiles. Caries Res 1983;17:385–391.
Ge J, Cui F, Wang X, Feng H: Property variations in the prism and the organic sheath within enamel by nanoindentation. Biomaterials 2005;26:3333–3339.
International tables for X-ray crystallography. Birmingham, Kynoch, 1962, pp 157–200.
Kielbassa AM, Wrbas KT, Schulte-Mönting J, Hellwig E: Correlation of transversal microradiography and microhardness on in situ-induced demineralization in irradiated and nonirradiated human dental enamel. Arch Oral Biol 1999;44:243–251.
Mahoney E, Holt A, Swain M, Kilpatrick N: The hardness and modulus of elasticity of primary molar teeth: an ultra-micro-indentation study. J Dent 2000;28:589–594.
Maj G: Ricerche statistiche sulla grossezza dei prismi dello smalto del dente umano. Arch Ital Anat Embriol 1947;52:186–192.
Oliver WC, Pharr GM: An improved technique for determing hardness and elastic modulus using load and displacement sensing indentation experiments. J Mater Res 1992;7:1564–1583.
Radlanski R, Renz H, Willersinn U, Cordis C, Duschner H: Outline and arrangement of enamel rods in human deciduous and permanent enamel: 3D-reconstructions obtained from CLSM and SEM images based on serial ground sections. Eur J Oral Sci 2001;109:409–414.
Reeh E, Douglas WH, Levine MJ: Lubrication of human and bovine enamel compared in an artificial mouth. Arch Oral Biol 1995;40:1063–1072.
Scott DB, Wyckoff RWG: Typical structures on replicas of apparently intact tooth surfaces. Public Health Rep 1946;61:1397–1400.
Spears IR: A three-dimensional finite element model of prismatic enamel: a re-appraisal of the data on the young's modulus of enamel. J Dent Res 1997;76:1690–1697.
Wilson P, Beynon AD: Mineralization differences between human deciduous and permanent enamel measured by quantitative microradiography. Arch Oral Biol 1989;34:85–88.
Young RA, Brown WE: Structures of biological minerals; in Nancollas GH (ed): Biological Mineralization and Demineralization. Report of the Dahlem Workshop. Berlin, Springer, 1982, pp 101–141.